SECOND SEMIANNUAL REPORT

NASA Grant NGR- 05-009-030

Physical Processes in the Magneto-Plasmadynamic Arc

March 1967

R. Lovberg, Principal Investigator

University of California, San Diego

La Jolla, California

SECOND SEMIANNUAL REPORT

NASA Grant NGR-05-009-030

Physical Processes in the
Magneto-Plasmadynamic Arc

March 1967

R. Lovberg, Principal Investigator
University of California, San Diego
La Jolla, California

Introduction

This report summarizes progress on NASA Grant NGR-05-009-030 during the first annual period March 1966-March 1967. We include herein material contained also in the first semiannual report.

During this year, our pulsed MPD arc facility has been constructed and put into operation. Considerable progress toward our goal of achieving a complete mapping of the electromagnetic field structure in the arc has been made; in particular, we have found that the discharge has the form of a spoke between anode and cathode which rotates with great regularity at a gyration frequency of typically 30 kc. These data (the field mappings) are still incomplete in many respects, and, furthermore, have been done only at one particular operating condition of the device. We have, however, made these first measurements at conditions which seem to be typical of those under which many D. C. devices are run.

A. System Design

A-1 Accelerator Design

The purpose of this program is to determine, as far as possible, the interior physical characteristics of an MPD arc which is itself representative of the arcs being investigated for possible thrust or application. Probes are to be our main diagnostic tool, at least initially, and thus, if these probes are to survive in the ~ 100 kw arc environment, the current flow must be held to short pulses. Short pulse operation also has the advantage that given a sufficiently large vacuum tank, the background pressure will not have a chance to rise significantly

even if the pumping system is slow; this, conditions more representative of a space environment can be maintained.

A caution which must be exercised when employing pulsed operation, however, is that a true steady state must be achieved during the pulse in order that the observed arc behavior may be taken as representative of D. C. devices. Voltage, current, gas flow, and field distributions must hold steady during a major part of the "on time."

We have selected 500 microseconds as a pulse length which is probably much longer than any typical MHD or electrodynamic time constants of the system, yet far shorter than the time it should take to harm a probe. During this time, moreover, there should be no returning pressure wave from the far end of our 8-foot tank, so a good vacuum should be maintained.

A half-millisecond is, however, far too short a time in which to heat the typical solid tungsten cathode to thermionic emission temperatures. For this reason, we have incorporated into our design concept a "flash-heated" cathode of thin tungsten sheet, which is brought to emission temperature in a fraction of a second just prior to the discharge.

In order that the interior of the discharge region might be mapped with acceptable resolution with realizable probes, it was decided to make the overall scale size of this device considerably larger than what might be called typical of MPD arcs. The geometrical configuration is also much simpler than usual. It was recognized that this departure carries with it some hazard of producing atypical arc operation, also; however, the design selected can be easily modified by simple electrode inserts in order to approximate existing arcs, and so the design was not regarded as too much of a gamble. (The ultimate justification for the design has

been, however, that quite representative MPD arc operation has been achieved, as will be described later.)

The final novel design requirement generated by our pulse mode is one for a fast-opening gas flow system which will establish a very uniform flow suitable for the arc in a time substantially shorter than two sonic transit times of the vacuum tank.

A-2 System Details

Figure 1 shows the accelerator structure, overall. The cylindrical anode is a stainless tube, 3.75 in. inside diameter, fitted tightly inside an alumina cylinder of 4.25 in. outside diameter which is cantilevered upon a nylon plate on the hinged cover plate of the vacuum tank. A narrow flange at the outer end of the anode supports a vacuum seal. The bias field coil, potted inside a slotted aluminum housing, rests near the end of the support insulator.

In Figure 2, the cathode and insulator can be seen. The cathode is a 1 cm wide band of 0.005" tungsten bent into a "hairpin", and clamped to the two halves of a split stainless steel support rod. The insulator performs the functions of: a) supporting the cathode structure and indulating it from the anode; b) providing a vacuum barrier between the discharge region and the atomopheric pressure region behind it; c) housing the gas supply system.

Figure 3 shows the insulator and gas supply system in full scale. The insulator is machined from "Mikroy," a type of ceramic made from a finely divided and compacted glass and mica mixture. Beneath the stainless plate which is cemented to its rear surface, there is an annular chamber

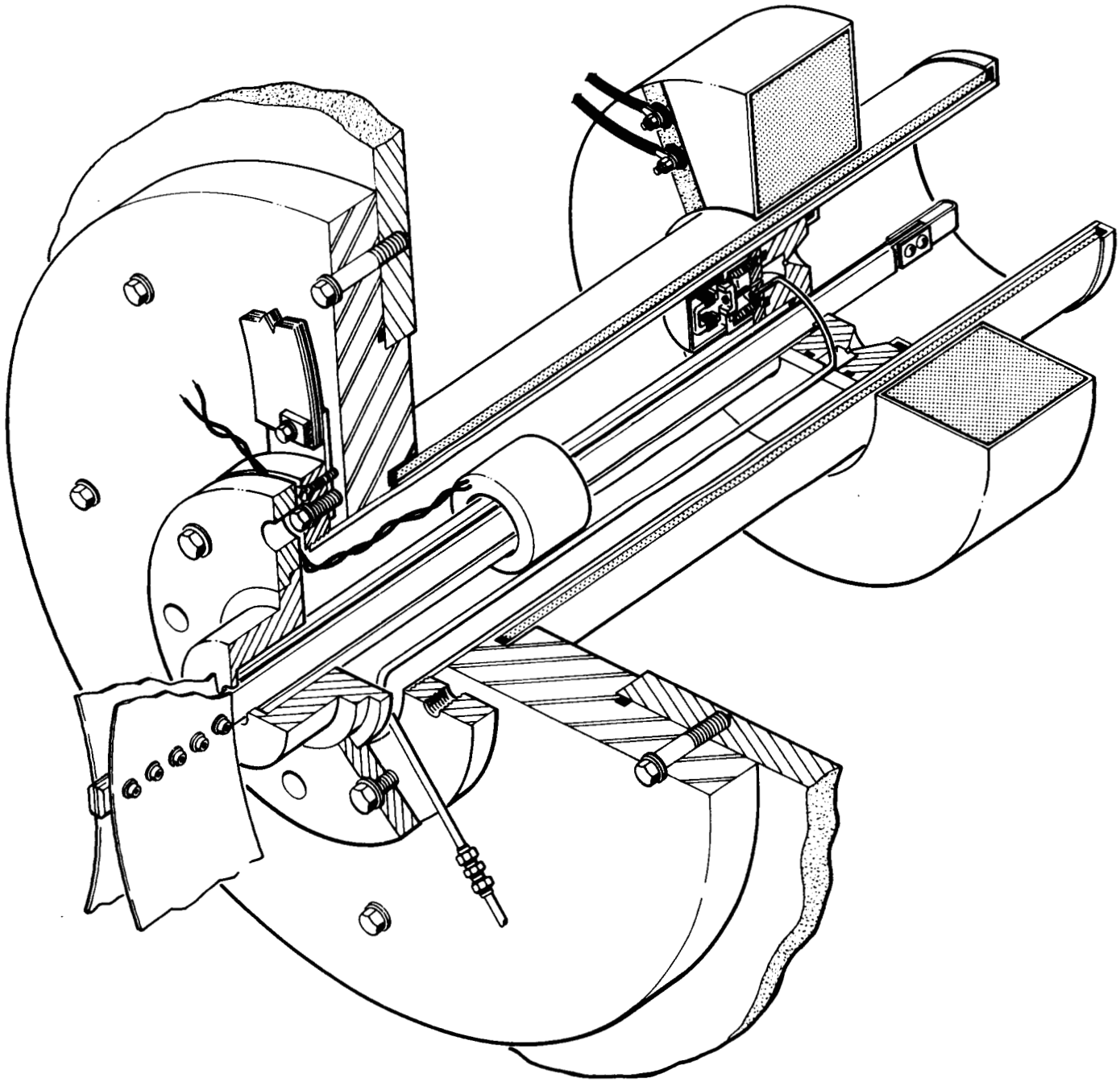

Fig. 1. Cutaway view of accelerator structure.

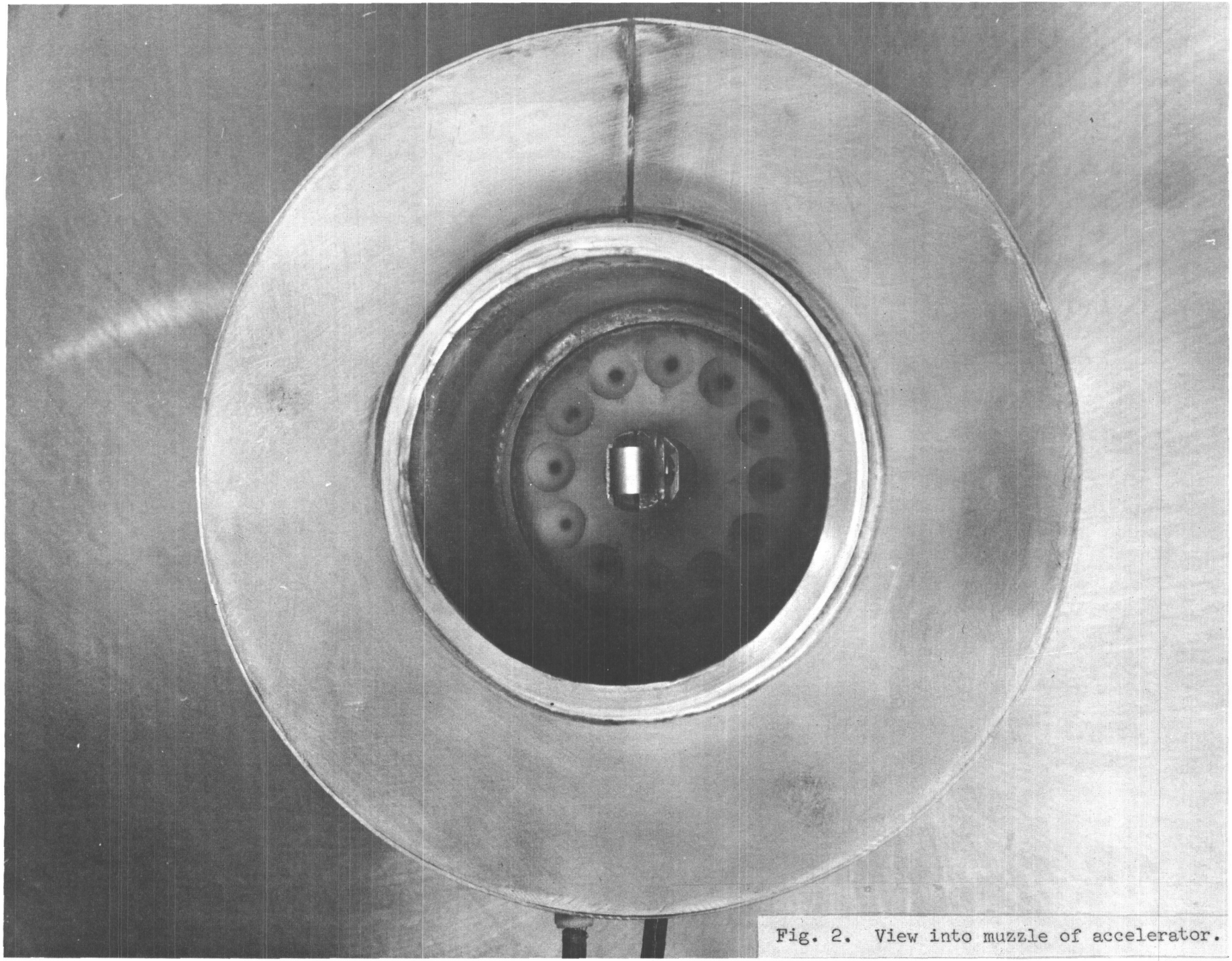

Fig. 2. View into muzzle of accelerator.

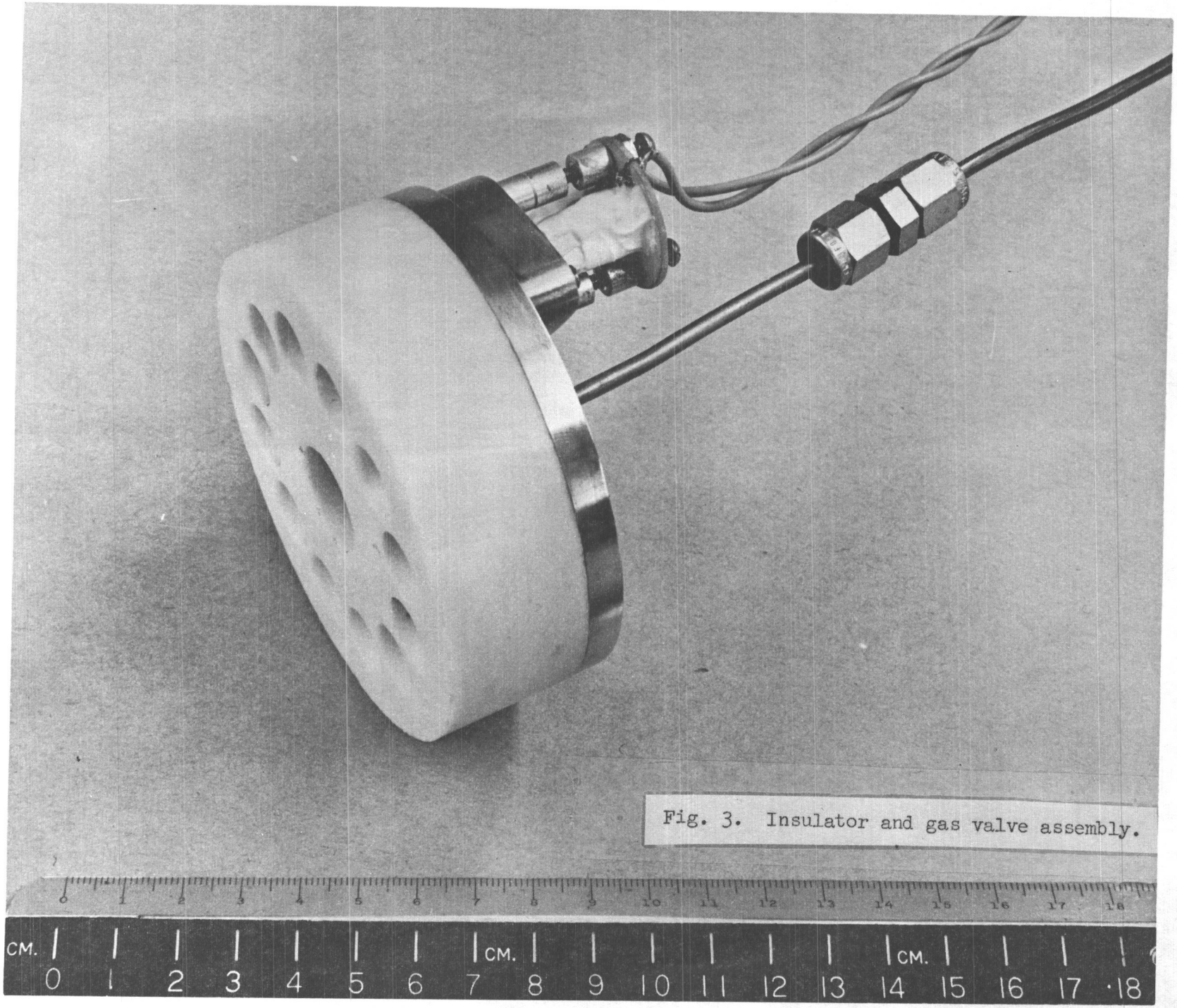

Fig. 3. Insulator and gas valve assembly.

of about 1 cm square cross section which feeds a set of twelve conical nozzles in the front face. Gas is dumped into the annular chamber from a small ($\sim$ 1 cm^3) high-pressure plenum by a very fast magnetic core valve. The valve, pulsed by a 20 volt, 10,000 microfarad electrolytic capacitor and SCR switch, achieves full opening in less than 200 microseconds.

The cathode assembly is shown in Figure 4. The two halves of the main supply conductor are cemented to a thin fiberglass separator, and potted inside an alumina sleeve. This structure achieves a vacuum seal against a step in the bore of the Mikroy insulator by means of the O-ring at the end of the alumina sleeve. It extends rearward beyond the main tank wall to a point where the main conductors from the cathode heating supply and discharge pulse supply bolt to the split rod.

This external connection area at the rear of the accelerator is seen in Fig. 5. The rectangular box on the table beneath the large flange contains a transformer which supplies the cathode heating pulse. With the cathode cold at the beginning of the pulse, approximately 200 amperes are drawn from the 220 volt primary line for two or three cycles; as heating progresses, however, the load resistance increases, and at the end of 0.3 to 0.4 seconds, the total load power, now balanced entirely by thermal radiation, is about 3kw. A welding-type SCR control circuit switches this primary power.

The aluminum straps which bring up the cathode heating power continue upward past the accelerator connection and are attached to one end of the secondary winding of the pulse transformer which rests on the top frame. Each of the two straps is actually bolted at this point to the

anode of a large silicon rectifiers; these two rectifiers have their cathodes tied together and to the transformer secondary. In this way, both sides of the cathode strap receive the main pulse current identically, since in this circuit, the two rectifiers are in parallel. Yet, as far as the A.C. heating pulse is concerned, the rectifiers are back-to-back, and so the two sides of the heating circuit are not shorted by their common connection to the pulse transformer.

The transformer itself has the function of matching the discharge impedance, which is in the 50 to 100 milli-ohm range, to the pulse forming network which serves as the energy source. It is quite difficult, in terms of component values, layout inductance, and switching, to build a 0.05 ohm, 100 volt pulse line, where an impedance of 5 ohms, for example, is almost trivially easy; thus, the transformer.

The transformer is wound on an o-core of 2-mil lamination thickness, which weighs about 40 pounds. The windings are made up of sandwiched 6-in. wide strips of 10-mil aluminum. The primary has 50 turns of two thicknesses each, and the secondary has 7 turns of 12 thicknesses. As can be seen in Fig. 5, the 12-layer secondary conductor is brought directly out from the transformer and bolted to the anode flange at the rear of the accelerator.

The 5-ohm pulse line has six sections, each with C = 8 μfd, and L = 200 μh, and can be charged to 4 kilovolts if necessary. An ignitron serves as the switch.

Energy for the bias field coil is supplied by a 200 microfarad bank which can be charged to 1 kilovolt. At present, the maximum field attainable is 2400 gauss.

Figure 6 is a general view of the entire installation. The vacuum tank is of 1/4" stainless steel, and is 4' i.d. and approximately 8' between the ends at the axis. The pumping system consists of a 140 cfm Stokes forepump and a 16" NRC oil diffusion pump with a liquid nitrogen chevron cold trap.

The relay racks contain vacuum controls (right bay) and power, control, and delay circuits for the accelerator are in the center bay. The pulse line and bias energy banks are also contained in these bays.

An externally controlled, hydraulically operated probe carriage is installed inside the tank in front of the accelerator position, and allows mapping in the r-z plane which includes the accelerator axis. A range of about 20 cm along either coordinate can be covered with the external controls. This carriage is seen in the general interior view of the tank, Fig. 7. The cylindrical object hanging from the tank ceiling in the foreground is a beam analyzer which has just been put into operation at the writing of this report.

A-3 Operating Sequence

Several functions, all transient in nature, must be carefully synchronized for proper operation of the accelerator. The actual sequence is the following:

1) The system firing switch activates the cathode heating pulser. A square switching pulse, variable in width between 0.1 and 0.5 seconds, is generated in this circuit, and is used in two ways. First, the pulse itself turns on the SCR which feeds 220 volt A.C. to the heater transformer; secondly, the drop to zero at the end of the pulse is differentiated to

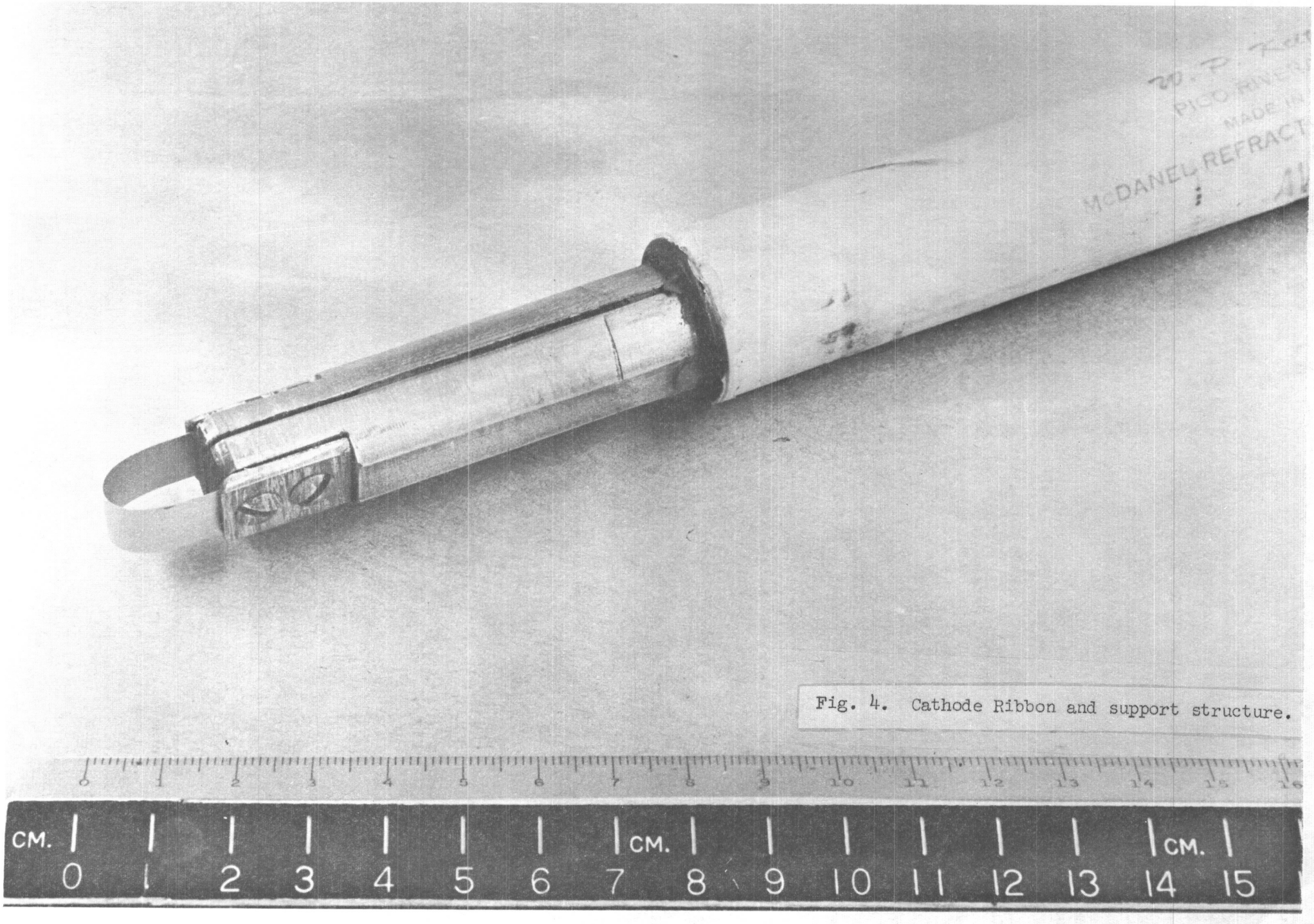

Fig. 4. Cathode Ribbon and support structure.

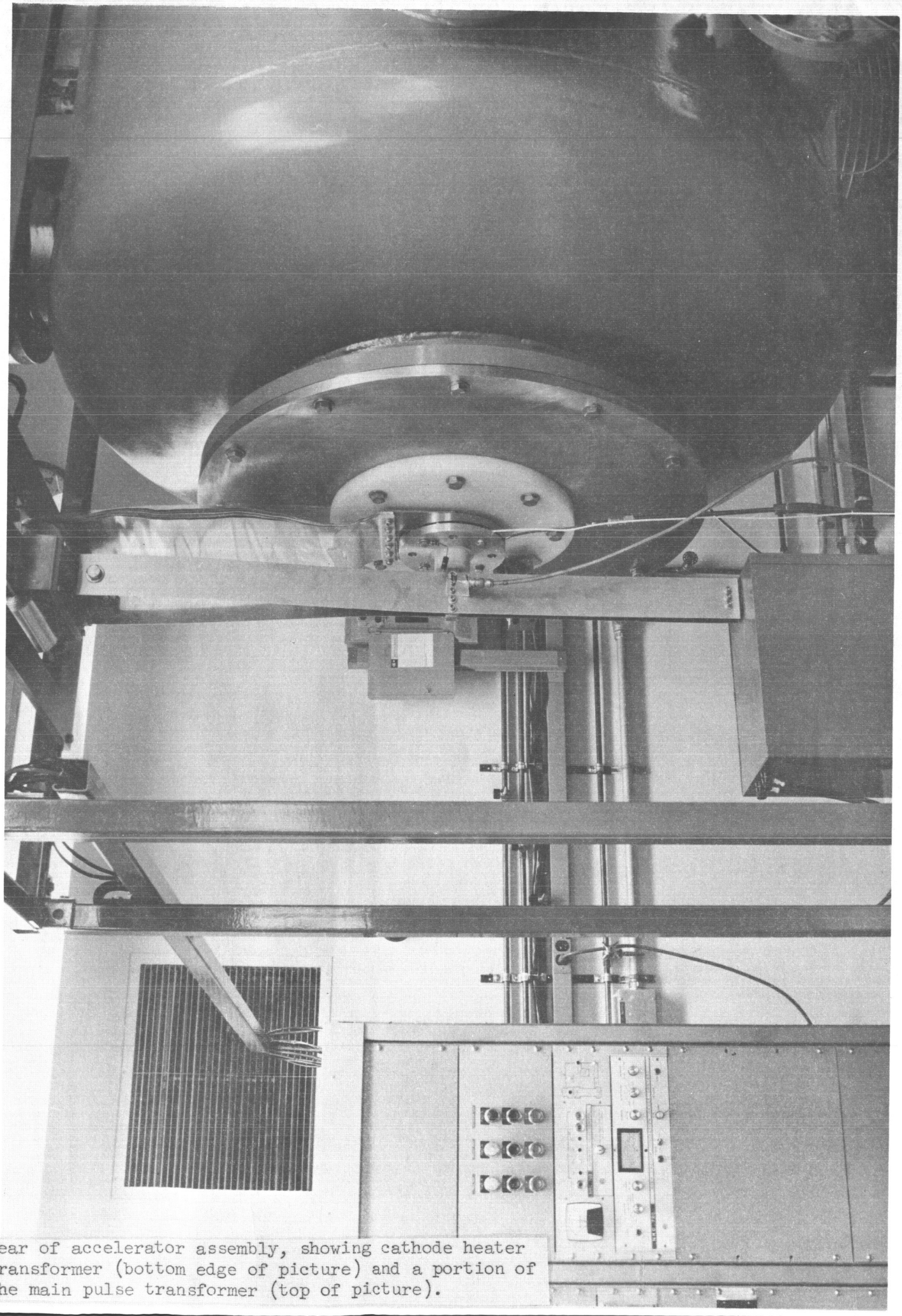

Fig. 5. Rear of accelerator assembly, showing cathode heater transformer (bottom edge of picture) and a portion of the main pulse transformer (top of picture).

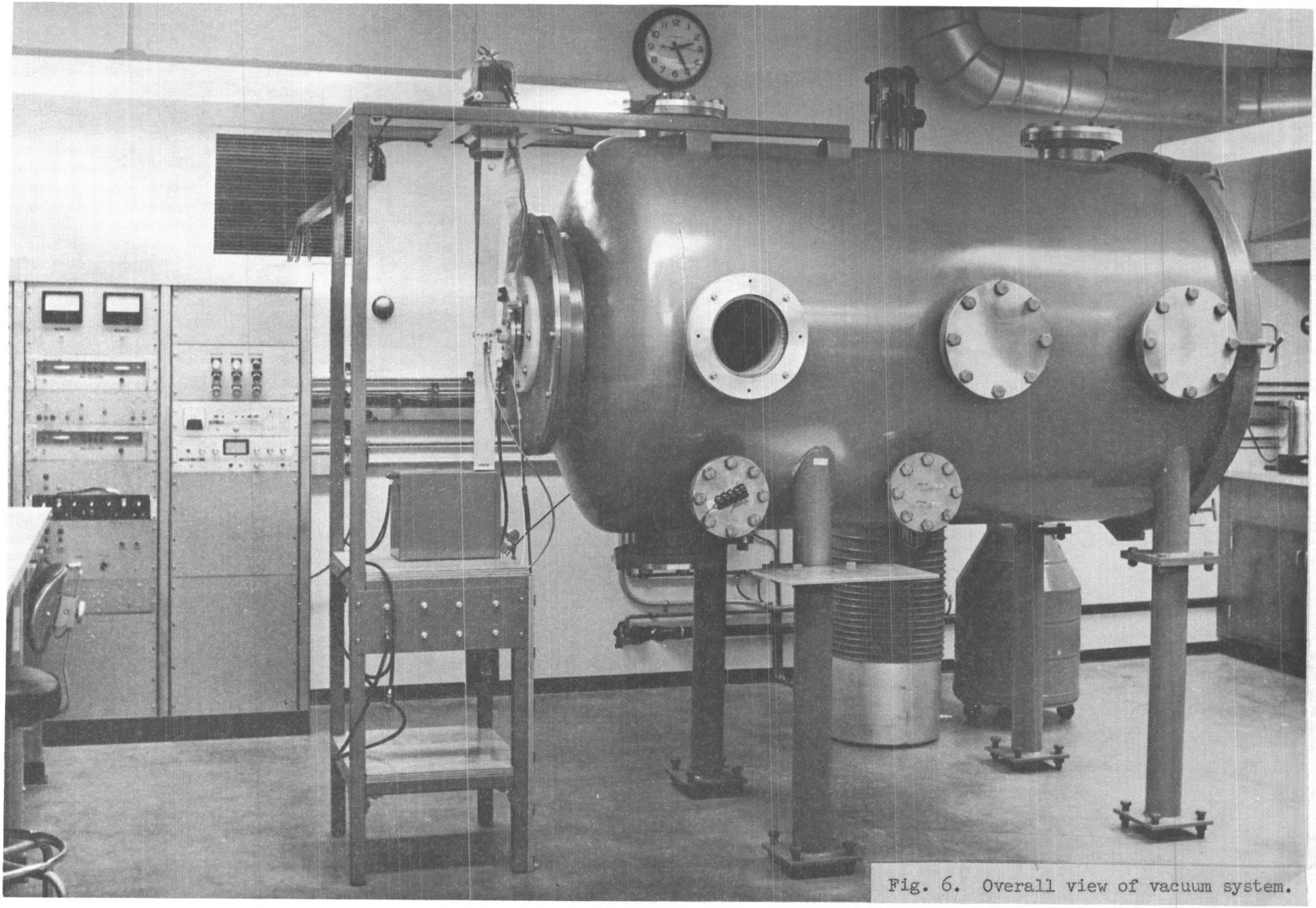

Fig. 6. Overall view of vacuum system.

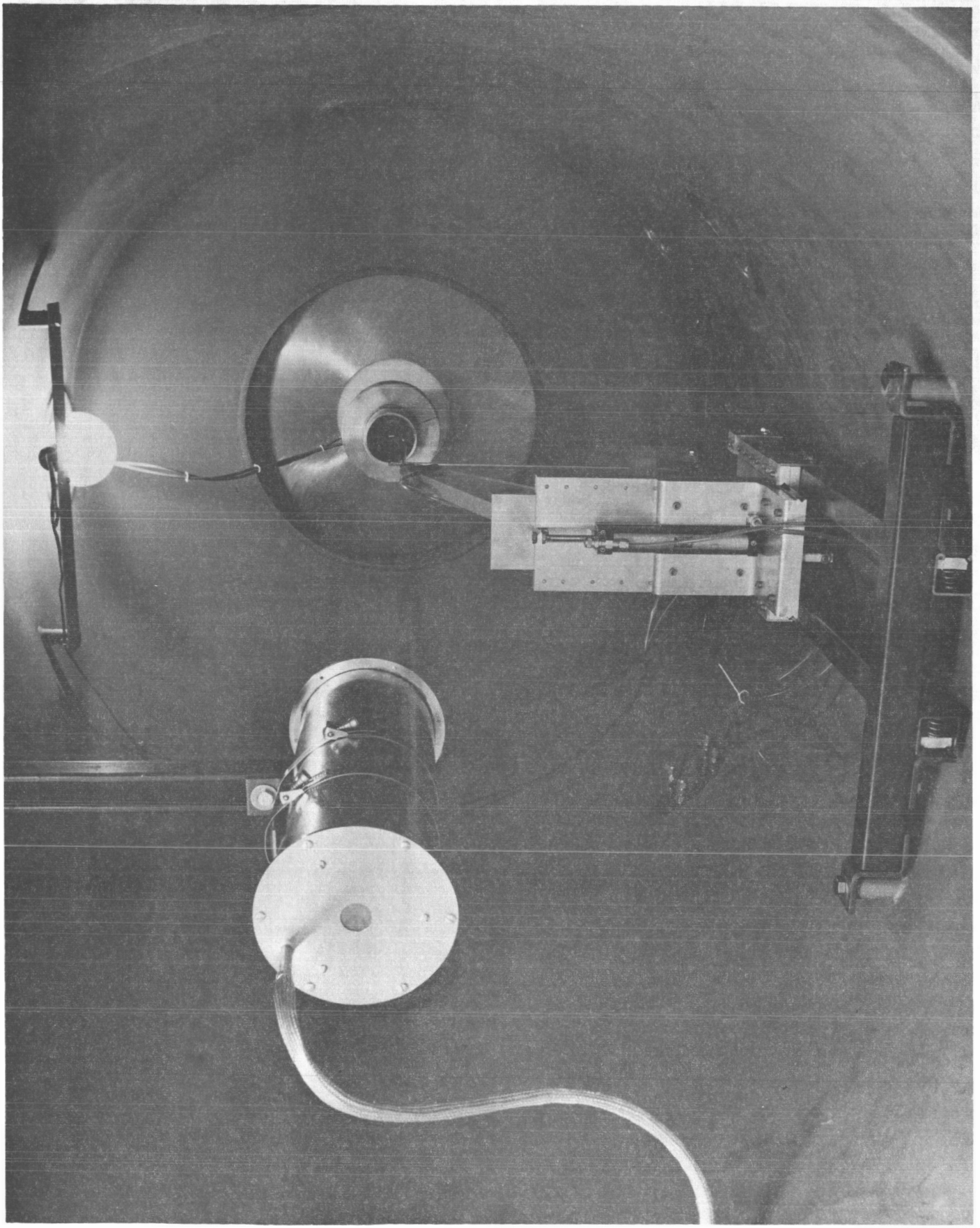

Fig. 7. Interior of tank. The structure on the tank floor is the two-axis hydraulic probe carriage. The electrostatic beam analyzer is in the upper foreground.

produce a timing fiducial which initiates all other events. Thus, the main system is fired at the instant the cathode heater is turned off. This works for the reason that the thermal decay time of the cathode (~ 0.5 second) is far longer than the entire time taken by the remaining events ($<10^{-2}$ s.), and so, the cathode is still effectively hot for the discharge, while possible modulation of system characteristics by the presence of high A.C. currents in the ribbon during the shot is avoided.

At this time also, a "reset" pulse is applied to the transformer core by means of a 3-turn tertiary winding and a low-voltage capacitor. This is necessary because the remenance of the core is high enough to result in a static core bias of several kilogauss after the unipolar pulse has passed. The reset pulse reverses this core bias, and makes available a total ΔB for the following pulse nearly twice as large as would have been possible for a core with no hysteresis.

2) The gas valve is opened.

3) After a delay of 1 to 10 milliseconds, (depending upon the propellant) the field coil pulse is switched on.

4) Exactly 2 milliseconds after the field coil is turned on (the field risetime), the main pulse line is fired.

Fig. 8 is an electrical schematic of the system, with the operating sequence noted.

A-4 External Measurements

The system was initially put into operation with argon used as a propellant; this gas has been used for all the data included in this report.

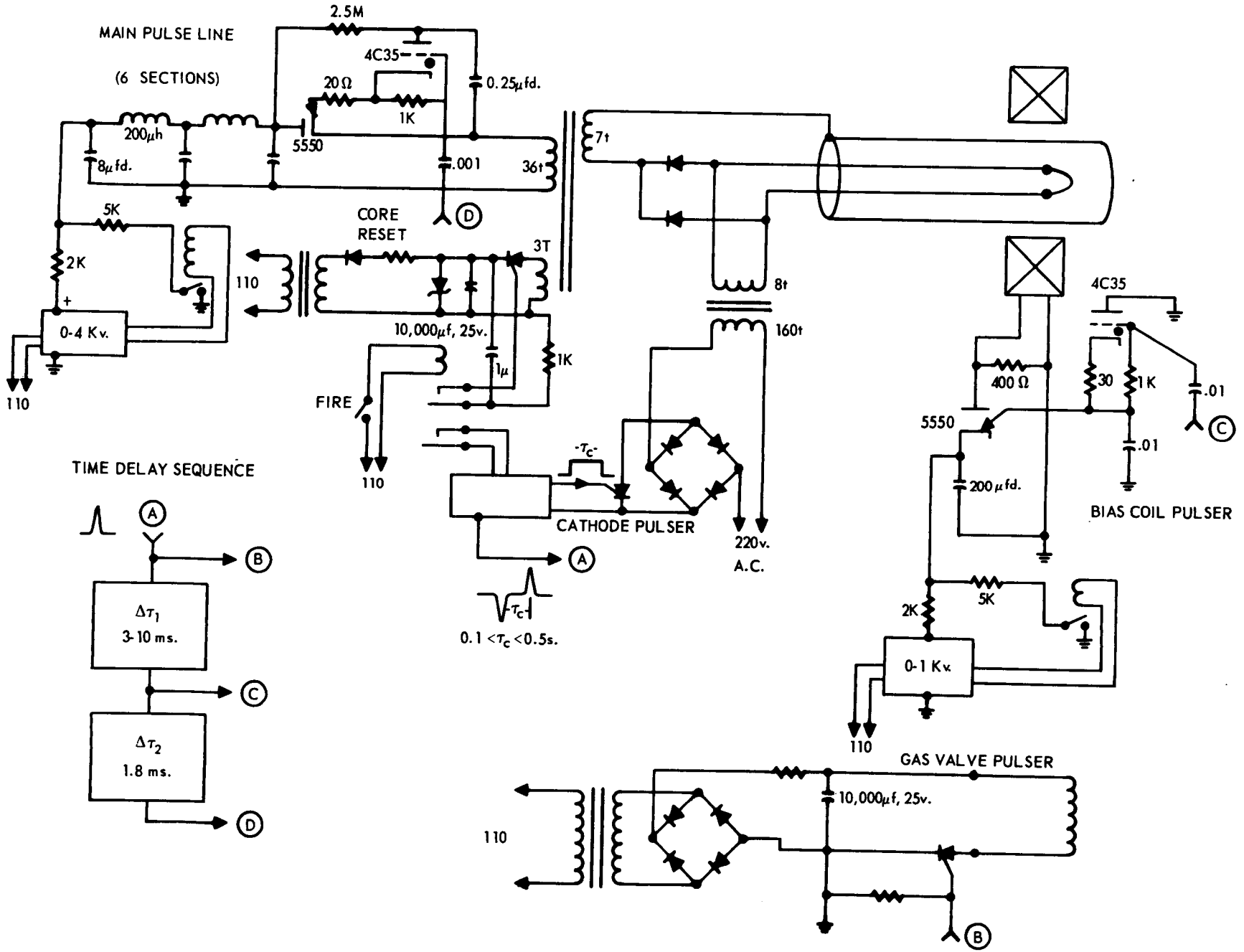

Fig. 8. Electrical schematic of system, with delay sequence at lower left.

It was found that because of leakage inductance in the transformer, the rise of the current to its steady value takes about 100 microseconds, and the decay to zero, beginning 400 microseconds later, also takes about 100 microseconds. However, the arc voltage jumps to its characteristic level almost immediately, and remains there until the decaying current is less than a tenth of its steady-state value. Fig. 9 shows a three-trace overlay of the voltage and current oscilloscope records for pulse line charging voltages of 2, 2.5, and 3 kv. It is plain that the voltage is completely independent of current for a given bias field. Fig. 10 is a plot of arc voltage and current for different bias fields, and a constant pulse line charging voltage of 1200 volts. We conclude, on the basis of these data, that this accelerator can be considered a typical MPD arc, at least in its electrical characteristics.

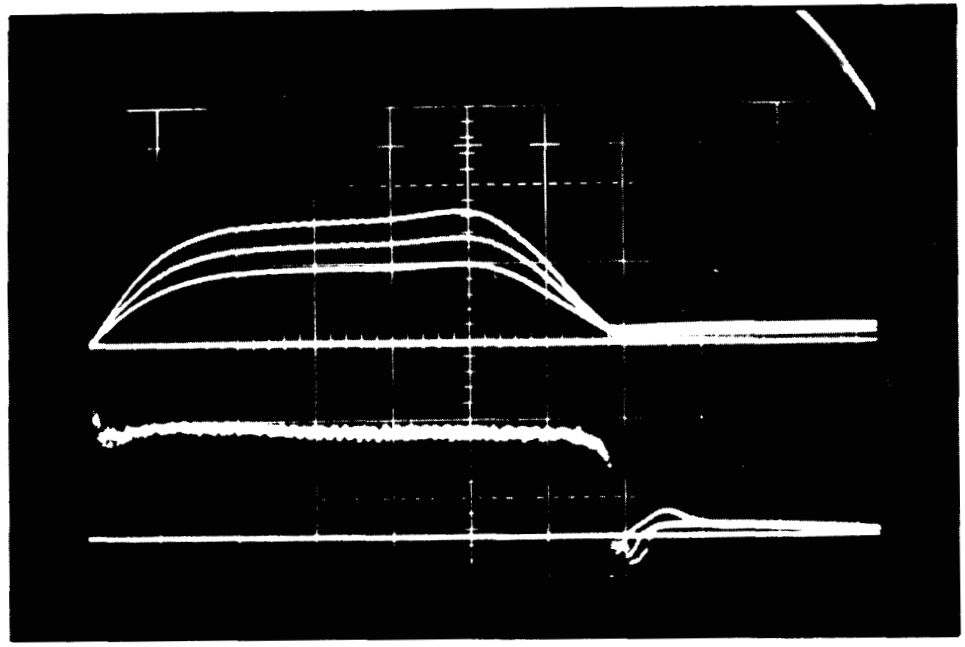

Fig. 9. Discharge current (upper traces) for line charging voltages of 2, 2.5, and 3 dv. Vertical, 1000 amperes/cm; horizontal, 100μs/cm.

Lower traces are discharge voltage (3 superimposed for the above charge voltages). Vertical, 50 v/cm.

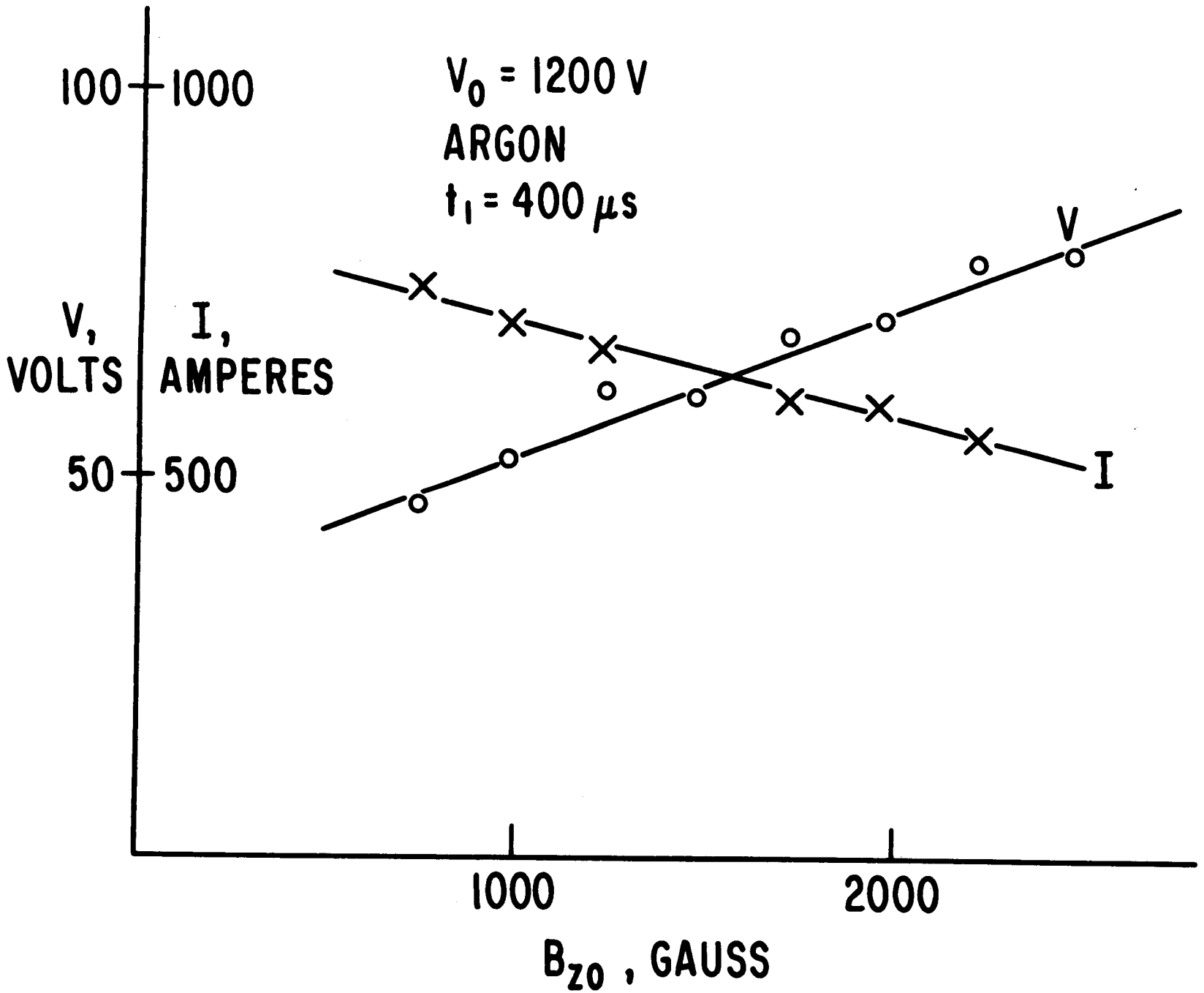

Fig. 10. Arc voltage and current as a function of applied axial bias field. B_{zo} is the field beneath the coil at z = 0, the rear insulator. (cf. Fig. 11). The pulse line voltage is 1200 v for all points.

B. Internal Diagnostics

B-1 General

During the recent semiannual period, the principal activity has been the mapping of the distribution of internal current and electromagnetic fields. A large fraction of the actual effort here has gone into the development of adequate probes; in some cases, this is a nontrivial problem, since the demands made upon the probes are somewhat more stringent than is the case for fast, high energy, impulsive systems, for example.

To specify this problem, one may consider magnetic field probes. In principle, we may determine the entire distribution of current within the arc by mapping the magnetic field and invoking Maxwell's equations. This is not simple for the MPD arc, however, because the azimuthal magnetic field B_θ , whose axial gradient is proportional to J_r , the radial current density, is at most 100 gauss under our typical operating conditions, while the axial bias field B_z is of the order of 2000 gauss. Since the bias field reaches its peak in only two milliseconds, and therefore has a frequency of the same order as that of the arc pulse, one cannot avoid the spurious B_z pickup which results from imperfect orientation of the B_θ probe by such stratagems as employing detection bandwidth appropriate for one field but not the other. On the other hand, the construction of a probe whose pickup coil axis is accurately enough aligned to make the B_z component negligible seems extremely difficult.

Our procedure here has been to construct a probe having two coils: one, oriented as well as possible in the θ direction, has the large number of turns necessary to yield an adequate output from the small transverse field, while the smaller second coil is wound over the first and oriented

to couple B_z directly. The two outputs are integrated separately by each of the two channels in a Tektronix Type O operational amplifier module, and then mixed in such polarity that the spurious B_z component from the θ coil and the output of the z-coil cancel each other. This is accomplished in a Tektronix 1A1 preamplifier in its differential mode. At each field point the nulling is first carried out by pulsing the bias coil alone, and adjusting the gain of the "trim coil" channel for zero baseline deflection. Any signal appearing during the main arc pulse will then be pure B_θ.

Problems of the same sort were encountered when "Rogowski coil" current probes were inserted into the discharge. When such a toroidal coil is used to measure, for example, the current in a wire which might be inserted through it, one finds that almost any coil works well in spite of imperfections in the distribution of the winding. However, there is also a requirement for a perfect null output when the coil is immersed in magnetic fields set up by currents <u>not</u> threading through it; this ideal behavior is only realized when the toroidal winding has perfect symmetry, and in particular no gaps such as usually exist at the connection point. Our application is particularly difficult in this regard, since, again, the self-field due to the plasma current is much smaller than the bias field. Despite quite careful construction, we have found it impossible to make a coil which ignores the bias field to the extent one would desire. However, by bucking this spurious output against the output of a current detector in the bias coil supply line, (using the mixing scheme described for the magnetic probes) we have been able to eliminate the extraneous component.

While we have employed a "parameter-variation" scheme in the initial exploratory experiments on this device, (principally to verify that it is actually an MPD arc in its voltage and current characteristics) it was deemed necessary to approach the internal field and current mapping experiments from an essentially opposite point of view, i.e., to adopt a single set of operating parameters -- voltage, bias field, propellant species and flow rate -- and to keep these constant throughout the entire series of probe experiments. This is obviously necessary if the various measurements are to be related in an intelligible way to one another. Once a complete set of measurements is in hand, it becomes sensible to go to some other operating condition; indeed, one would at this point probably be able to make a very well-reasoned choice of new parameters.

Our initial choice of "standard" conditions is, then, the following:

$$V = 75 \text{ v.}$$

$$I = 550 \text{ a.}$$

$$B_{zo} = 2200 \text{ gauss}$$

Propellant: Argon

We are not yet certain of the propellant flow rate and pressure because the gauges employed initially (fast ion gauges or hot-wire anemometers) proved to be unreliable due to severe nonlinearity (ion gauge) or sluggish transient response (anemometer). It is possible to make a rough estimate, however, from our knowledge of the total amount of gas admitted per shot, and the duration of the flow as indicated by the otherwise erratic fast ion gauge. On such a basis, we estimate the flow rate during the discharge to be on the order of 0.1 g/sec.

B-2 B_θ Measurements

The first attempts at internal mapping were done with a B_θ-oriented probe which was compensated for B_z pickup, as described previously. In all the following discussions of spatial distributions of various quantities, we employ the coordinate system shown in Fig. 11. Z = 0 is the rear insulator, Z = 7.5 cm is the cathode tip, and Z = 10.5 cm is the edge of the anode. The main cathode support rods have a radius of 1 cm., and R = 4.4 cm is the inner wall of the anode.

The bias field coil is centered just over the rear insulator at Z = 0, and the nominal value of the field, B_{zo}, is its strength at this position. Fig. 11 shows some representative values of the z-component of the bias field at other points in the inter-electrode region.

The earliest B_θ records which were obtained yielded clear evidence for the most characteristic and dramatic feature of the operation of this arc, namely the rapidly rotating, azimuthally nonuniform current distribution. In Fig. 12 are shown two pairs of $B_\theta(t)$ records, taken at Z = 1.5 cm (near the rear insulator) and Z = 5.5 cm, which is close to the tip of the cathode. The radius was 2 cm.

Average B_θ during the 600 microsecond pulse is the same at both axial positions, indicating that there is negligible radial current flow between them; however, the strength of the rather pure high frequency modulation is markedly stronger near the muzzle. This would occur naturally if the current between electrodes were mainly confined in a radial spoke which undergoes rapid azimuthal rotation.

The rotation hypothesis was tested by the use of a pair of B_θ probes which were placed at the same r and z, but 180° apart in azimuth. The high frequency components indeed displayed a 180° relative phase shift.

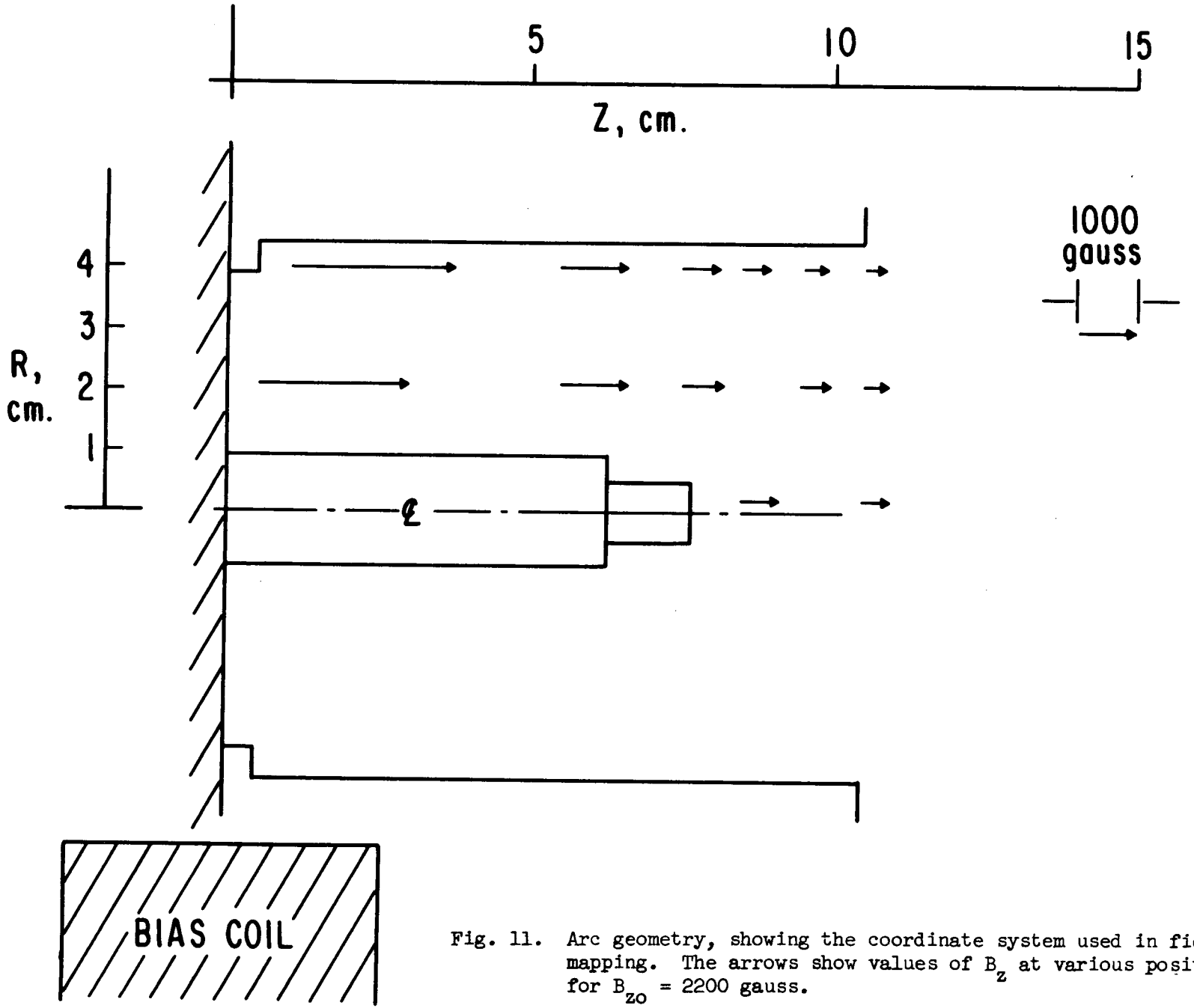

Fig. 11. Arc geometry, showing the coordinate system used in field mapping. The arrows show values of B_z at various positions for B_{zo} = 2200 gauss.

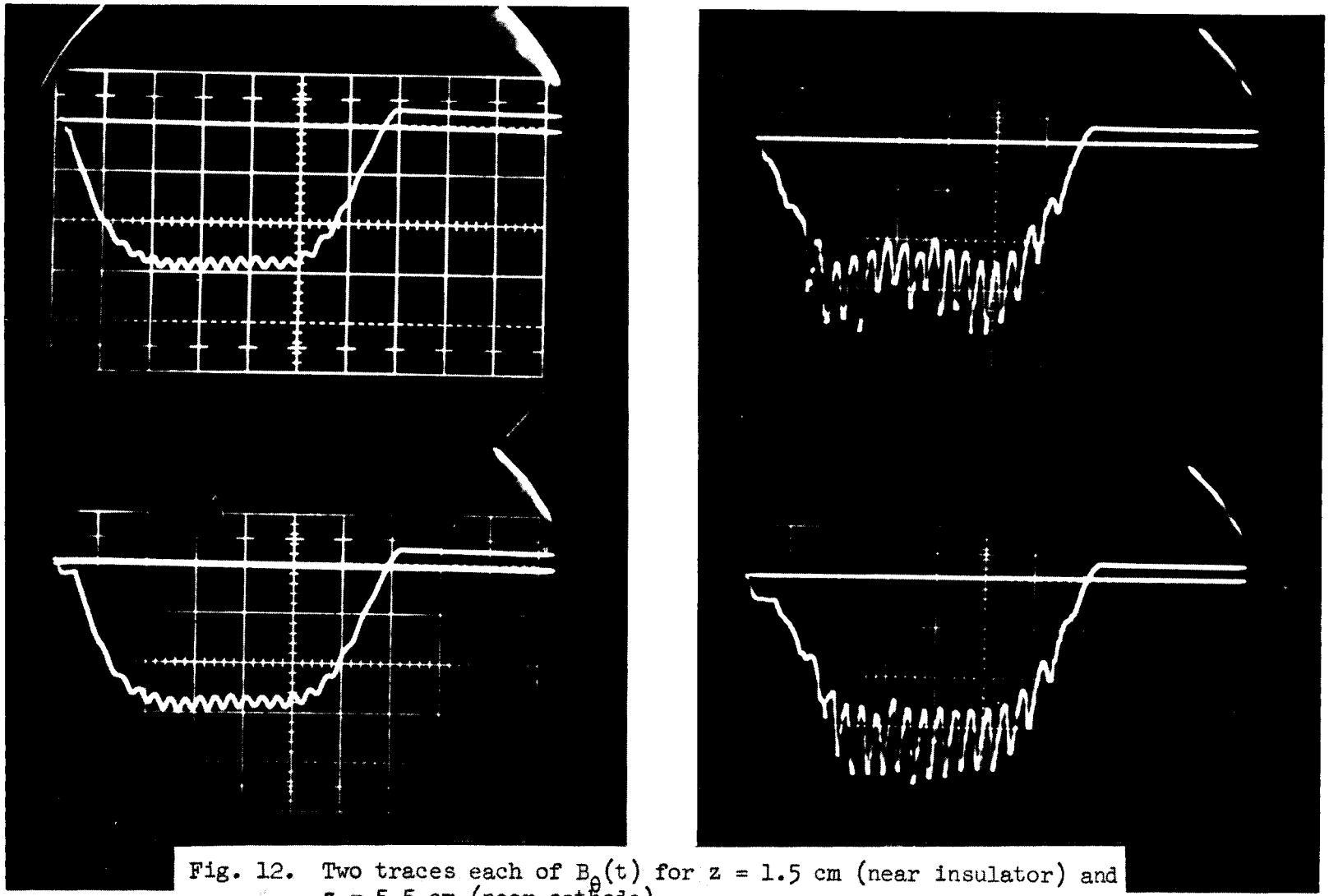

Fig. 12. Two traces each of $B_\theta(t)$ for z = 1.5 cm (near insulator) and z = 5.5 cm (near cathode).

Z = 1.5

Z = 5.5

B_θ at r = 2 cm

B-3 Rogowski Coil Current Measurements.

Initially in this program, it was hoped that mapping of $\vec{B}(r,z)$ would suffice to allow a specification of the total current distribution. Such a possibility rests largely upon the assumption that the discharge is azimuthally uniform, for then,

$$\mu_o \vec{J} = -\frac{\partial B_\theta}{\partial z}\hat{r} + \left[\frac{\partial B_r}{\partial z} - \frac{\partial B_z}{\partial r}\right]\hat{\theta} + \frac{1}{r}\frac{\partial}{\partial r}(rB_\theta)\hat{z} \quad ,$$

and while the combination of four terms from three separate two-dimensional mappings is somewhat cumbersome, it is manageable. The appearance of a rather extreme azimuthal nonuniformity adds two more terms to the curl $\vec{B}$ equation, and requires three-dimensional mappings of all three components, which would be extremely difficult to accomplish and to coordinate.

In the face of this situation, it was decided to employ Rogowski coil probes in order to measure current densities directly. The ordinary objection to the use of such probes in a plasma system is that they are intrinsically more cumbersome than B probes, and accordingly, have poorer spatial resolution as well as presenting a larger perturbation to the plasma. However, in this instance, these disadvantages appeared to be outweighed by the single advantage of obtaining a fairly direct, if somewhat approximate, determination of the current flow pattern.

Initial surveys were done with a coil having an open circular aperture 2.5 cm in diameter, and a minor cross section of the torus of about 4 mm. (It seems reasonable to expect that if the aspect ratio of the coil, i.e.,

the ratio of major to minor diameter, is large, the current flow actually measured should suffer minimal perturbation.) The problems of constructing a well-balanced, or evenly distributed coil with minimal feedpoint error consumed a fair amount of time here. Finally, a mixing scheme was used to cancel out stray bias field components, as described earlier, although this large 1-inch coil suffered from imbalance much less than did later, more compact units.

It was found by the use of this sensor, then, that the current flow is indeed sharply localized in azimuth. Fig. 13 is a set of integrated Rogowski coil signals of J_r taken at two different radii, one near the cathode and the other near the anode. Seven values of z are covered. The sweep speed used in this presentation is 10 μsec/cm, with the scope sweep delayed until steady-state conditions have been achieved; the sweep delay used here is 300 μsec. Since the shot-to-shot phase of the plasma rotation is random with respect to the initial trigger pulse, the phase differences between these pictures have no significance.

Several points are obvious from these photos, however. First, one sees that at r = 3.5, (~ 1 cm from the anode) the current is highly localized in both z and θ, i.e., it is a thin spoke, which connects to the anode in the vicinity of its lip at z = 10.5 cm. The rotation rate is extremely regular at about 31 kc. Nearer the cathode, the flow is spread out considerably, both in z and θ, although by taking the r-oriented coil to r = 1.5 (actually, the distance between the coil plane and the axis) we have reduced its θ-resolution to about 80°, and so, must attribute some of the apparent azimuthal spread to this instrumental effect. In this instance, one sees the radial current flow extending from about the cathode tip to at least 2 cm past the anode.

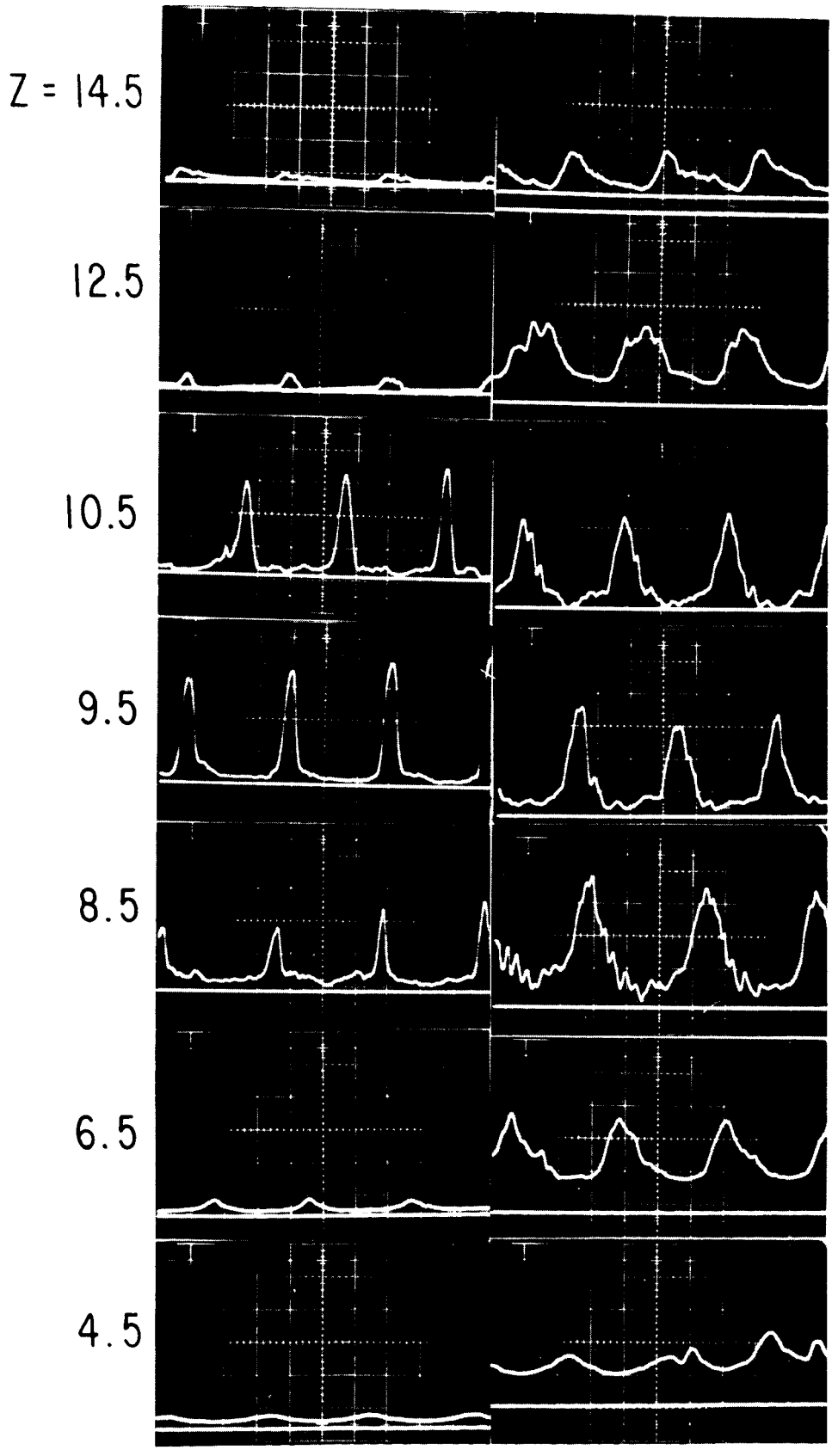

Fig. 13. $J_r(t)$ traces for various r and z. The phase differences between different traces are not significant (see text).

We have used the Rogowski coil to insert one additional set of "parameter studies" before continuing on with the detailed probing; these are measurements of the rotation frequency as a function of bias field and current. Since it seems obvious that the rotation of the spoke is driven by $\vec{J} \times \vec{B}$, the frequency can be expected to have some dependence upon the imposed current and bias field. As can be seen from Figs. 14 and 15, this dependence exists, although it is not extremely simple. It is reasonable that this should be so, since variation in either the total current or B_{zo} has the likely effect of moving the axial position of the discharge, thus re-distributing the current, and in particular, changing the fraction of B_{zo} which represents the effective field strength in the spoke.

B-4 Phase-Triggered Data Presentation.

With the appearance of the spoke-like distribution of discharge current, it became evident that various mappings of such parameters as $\vec{E}$, $\vec{B}$, and $\vec{J}$ could never be correlated unless there were a possibility of relating their relative azimuthal phases. It is clear that if, for example, the data from a given probe exhibits a sufficiently uniform oscillatory behavior with spoke rotation, we can immediately relate its time phase as displayed on the oscillograms of Fig. 13, for example, to the azimuthal coordinate, θ. In other words, the uniform rotation of the distribution has presented us with a free gift of a full three-dimensional mapping even though the probe carriage moves only along r and z.

The trouble is that, as mentioned before, the rotation phase is random with respect to the beginning of the pulse, and so, with the recording oscilloscope triggered by the line firing signal, there is no

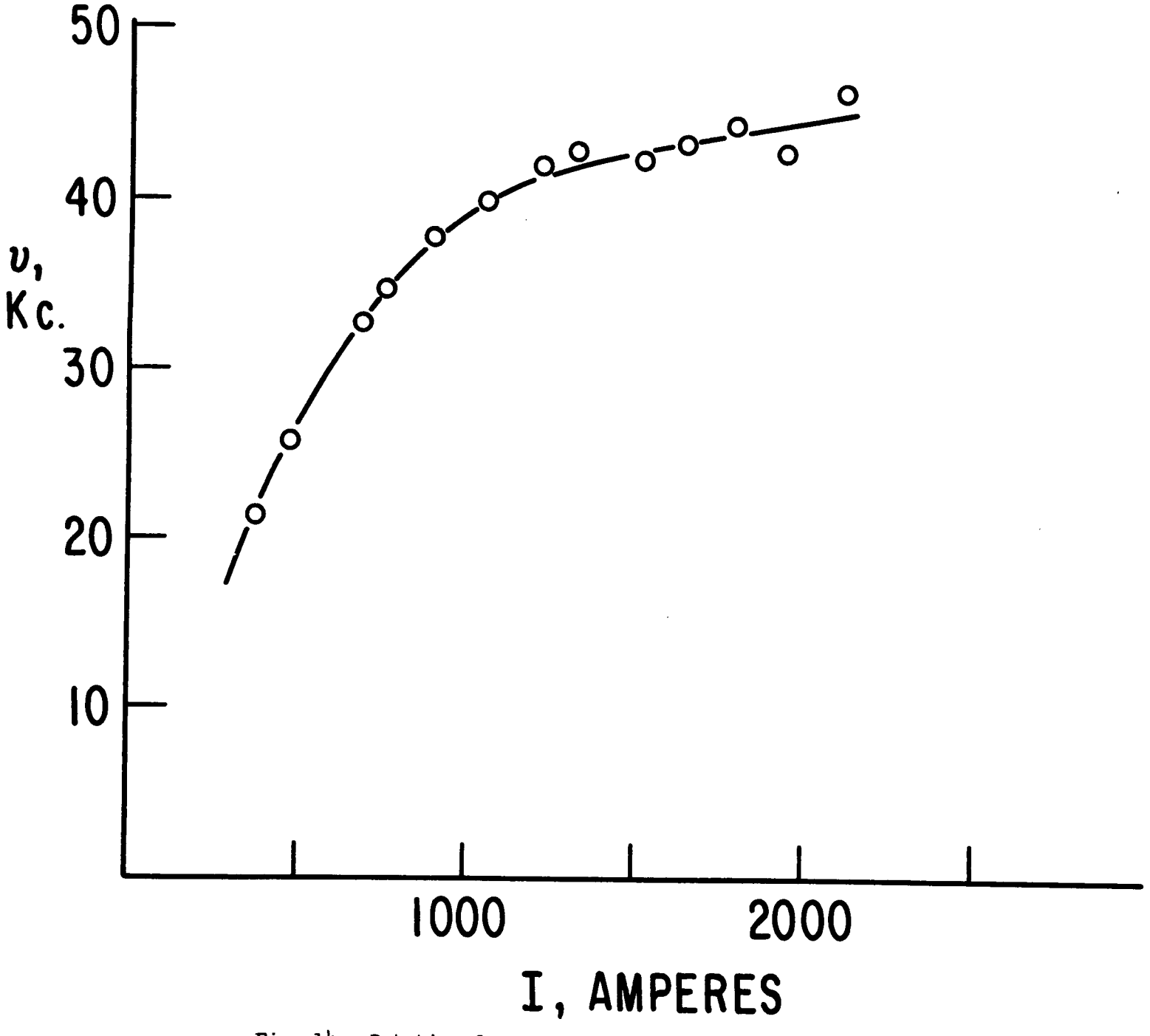

Fig. 14. Rotation frequency as a function of arc current. B_{zo} = 2200 gauss.

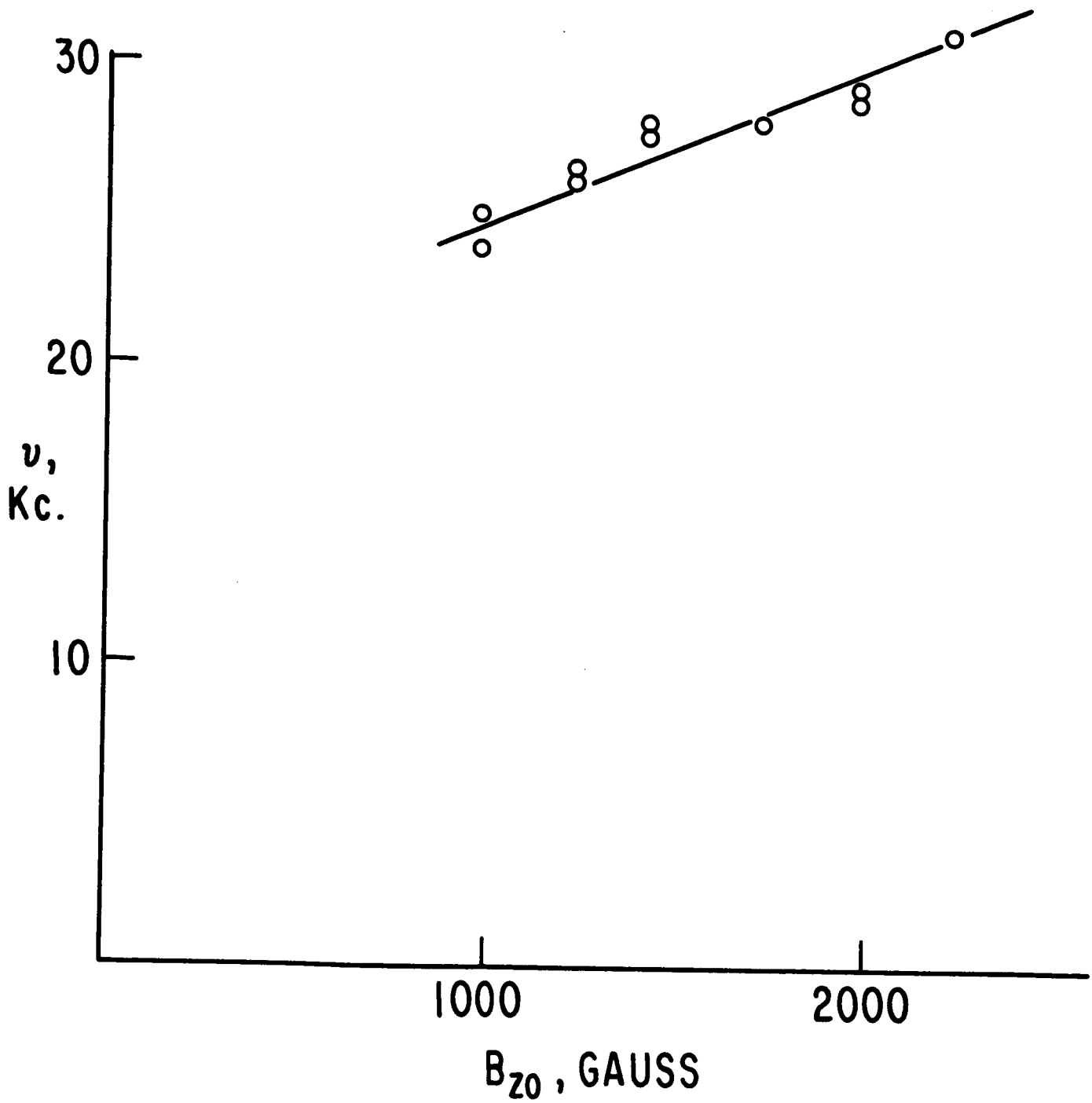

Fig. 15. Rotation frequency as a function of B_{zo}.

hope of comparing the relative θ displacements of data taken on successive shots of the machine.

We have overcome this difficulty by the expedient of using a permanently installed "phase reference probe" to act as the oscilloscope trigger. This B_θ coil is mounted just outside the anode lip, as seen in Fig. 16. Its unintegrated output is ideal for this function, since it is an extremely short spike which appears each time the discharge spoke passes. This trigger mode carries the further singular advantage that the scope can be swept on every rotation, or every other rotation of the current, (depending on sweep speed) and thus, we obtain an overlay of many data traces on a single shot of the machine.

It is obviously desirable, however, that this multi-trace recording be done only during that portion of the pulse when the discharge is in its steady state. To meet this criterion, we have employed a delayed gating of the oscilloscope z-axis (beam intensity) so that, in a typical instance, only the traces triggered during the second 200 μsec of the pulse are recorded.

We are enabled also, by the use of this scheme, to assign to the azimuthal distributions a probable error based upon the cycle-to-cycle scatter in the data. With as many as eight traces appearing in some records, the assignment of this "scatter error" can be done with some confidence.

Fig. 17, which presents $E_\theta(\theta)$, a measurement to be discussed below, is a sample of data taken in this way. We will first mention certain current measurements, however.

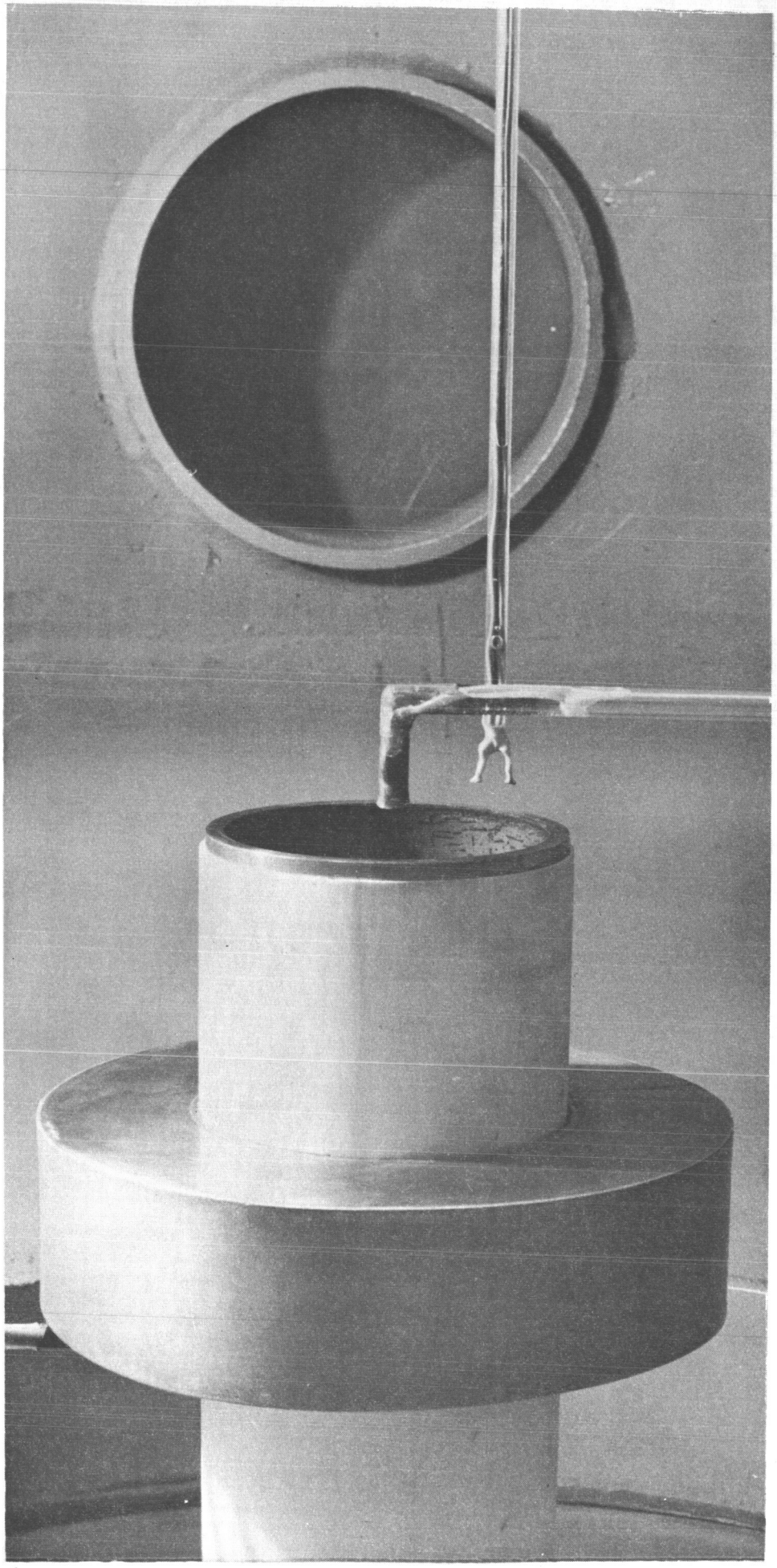

Fig. 16. Muzzle region of accelerator, showing phase reference probe (L-shaped), together with differential E-probe.

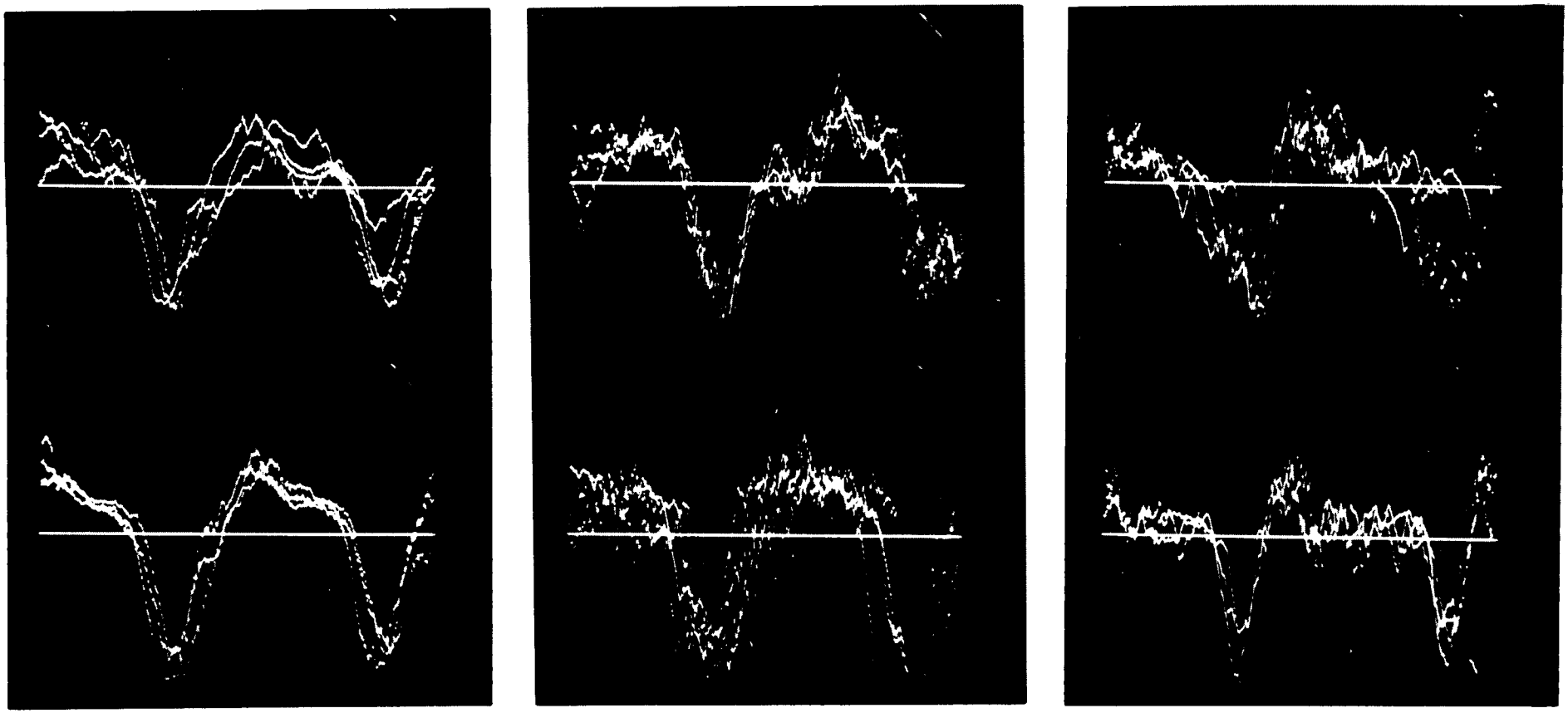

Fig. 17. $E_\theta(t)$ in region of rotating spoke. Phase-probe triggering allows multiple-overlay data from single arc pulses.

B-5 Spatial Distribution of J_r.

The phase-triggering scheme allowed an investigation into the question of whether the current spoke, or current "fan", as implied from the data of Fig. 13 lies in the r-z plane, or whether, as some models of its behavior might suggest, it has the form of a spiral as seen from the front.

We have found that the current peak is in fact in an r-z plane, i.e., that there is no observable phase difference in the current density as the Rogowski coil is moved along r or along z.

In order to look for a spiral current structure in another, and perhaps more sensitive way, we examined the Rogowski coil output with its orientation in the J_θ direction. (The toroidal coil lay in the r-z plane, with its major axis along θ.) If the current spirals, one expects to observe a momentary pulse of current in one direction each time the spoke sweeps over the coil, this pulse corresponding to the θ-component of the current spiral pattern. What was actually observed was a positive pulse immediately followed by a nearly identical negative pulse, with the zero crossover occurring at the phase of the current maximum for J_r. This result is easily interpreted as meaning that the current maximum lies along a radius (no spiral), but that the channel fattens out rapidly for smaller radii, thus introducing azimuthal components of opposite signs on opposite sides of the peak. This result is nicely consonant with the results of Fig 13, also.

At this point, we draw a significant conclusion: This MPD arc carries no azimuthal current, contrary to the widely held view that azimuthal "Hall current" is the principal agent for accelerating MPD arc plasmas.

Our determination of the details of current flow is incomplete, however, since we have not yet measured J_z. The Rogowski coil for this purpose has just been made, but no measurements have been done.

B-6 Azimuthal Electric Field, E_θ .

The azimuthal electric field E_θ is of fundamental interest in the MPD arc because, in particular, it cannot exist in a steady state discharge which is azimuthally uniform. This follows simply from Faraday's law, which, as the integral form of Maxwell's curl $\vec{E}$ equation, says that

$$\oint \vec{E} \cdot d\vec{\ell} = -\frac{\partial \phi}{\partial t} \quad ,$$

where ϕ is the total magnetic flux through the contour around which E is integrated. If the integration contour is a circle of radius r surrounding the axis, this becomes

$$\int_0^{2\pi} E_\theta \, d\theta = -\frac{1}{r}\frac{\partial \phi}{\partial t} \quad ,$$

which must equal zero for steady state even if $E_\theta(\theta)$ is not uniform. With azimuthal symmetry, however, E_θ must be equal for all θ, and so, must be identically zero.

The trouble with $E_\theta = 0$ is that this condition does not allow the electrons to carry the main discharge current regardless of the value of ωt, the Hall parameter. We reason that the aximuthal force $J_r B_z$ applied to the plasma is applied directly to the electrons, and thus, the azimuthal momentum transfer to ions must occur either through an azimuthal E_θ (not permitted) or through a direct viscous drag. But an azimuthal drag upon ions by electrons is itself a resistive current flow which must be accompanied by an E_θ - again not permitted. It is therefore a necessary consequence of $E_\theta = 0$ that ions must carry a fraction of the total radial current equal to their fraction of the total mass density, i.e., nearly all of it.

If the system is not azimuthally uniform, however, we need only meet the requirement that

$$\int_0^{2\pi} E_\theta \, d\theta = 0$$

which allows for local departures of E_θ away from zero, and thus allows radial electron current to flow.

We measure $\vec{E}$ in the plasma by using the differential floating probe technique, in which a pair of electrodes is exposed to the plasma at two neighboring points, and the difference in their floating potentials is recorded. As an approximation, we assume that the difference in floating potential is also the difference in space potential; the error in this assumption is due to whatever difference in electron temperature there may be between the two electrodes, since

$$V_f = V_{sp} - \alpha k T_e ,$$

so

$$\Delta V_f = \Delta V_{sp} - \alpha k \Delta T_e$$

Now α is usually in the neighborhood of 3 or 4, and so, for a plasma temperature of lev, for example, αkT_e could amount to 3 or 4 volts. In an extreme case of an electron temperature gradient of 1 ev/cm or more, and an actual electric field of less than 5 v/cm or so, the assumption that $\Delta V_f = \Delta V_{sp}$ is not a good one; however, it is very unlikely that we encounter temperature gradients this large except at the walls, and, additionally, the local electric fields are usually larger than 5 v/cm.

Fig. 17 shows $E_\theta(t)$, which converts directly to $E_\theta(\theta)$, for three radii. These curves are seen to repeat rather well from one rotation cycle to another, and it is clear that they integrate very nearly to zero over a cycle.

We may make a rough estimate of electron density here, if we also insert the assumption that electrons carry the entire current. In such an instance, the azimuthal force per unit volume is applied to the ions by the E_θ field, and since the ions contain nearly all of the plasma mass, this force is equal to $\vec{J} \times \vec{B}$ on the electrons. Thus,

$$n_i e E_\theta = J_r B_z \quad ;$$

We set $n_i \simeq n_e$, and neglect the additional term $J_z B_r$, which is suitably small in certain regions. Then,

$$n_e \simeq \frac{J_r B_z}{e E_\theta}$$

At z = 10.5 cm, and r = 3 cm, approximate values of the field quantities are:

$$B_z = 400 \text{ gauss}$$

$$J_r = 200 \text{ amperes/cm}^2$$

$$E_\theta = 5 \text{ v/cm}$$

These yield

$$n_e = 10^{15} \text{ cm}^{-3}$$

B-7 Spatial Potential Distribution

In order to obtain, for a particular azimuth, a two-dimensional representation of the electric field in the r-z plane, we have employed a single-electrode floating probe, and made contour maps of potential (floating), from which electric fields can be inferred. Figures 18 and 19 are such maps, the first being taken at the azimuth of the current spoke, and the second, 180° away. It appears that (not unexpectedly) the equipotentials lie approximately along the magnetic field lines. Of particular significance is the actual level of potential within the interelectrode region. The contours are labeled with their potentials with respect to the cathode; one can see that in the region where the current flow occurs, these are generally less than 50 volts, and yet a total of 80 volts is applied between the electrodes. It is plain that there is a thin sheath, dropping about 30 volts, over the anode. Nearly 40% of the input power is thus dissipated in this narrow region.

B-8 Beam Analysis

Work has just begun on analysis of the downstream plasma by means of a gridded electrostatic particle analyzer. This device consists of an array of 12 "pinhole" apertures, followed, after a suitable plasma expansion distance, by a negatively charged fine-mesh grid which separates out plasma electrons, and then a coarse secondary emission suppressor, and a biased collector plate, in order.

In preliminary tests, this analyzer was placed 1.6 meters from the muzzle of the accelerator and produced an output nearly identical in shape to the current pulse in the arc, but displaced 200 microseconds in time, implying a plasma velocity of about 0.8 cm/μsec, which corresponds to a kinetic energy of about 13 ev for argon.

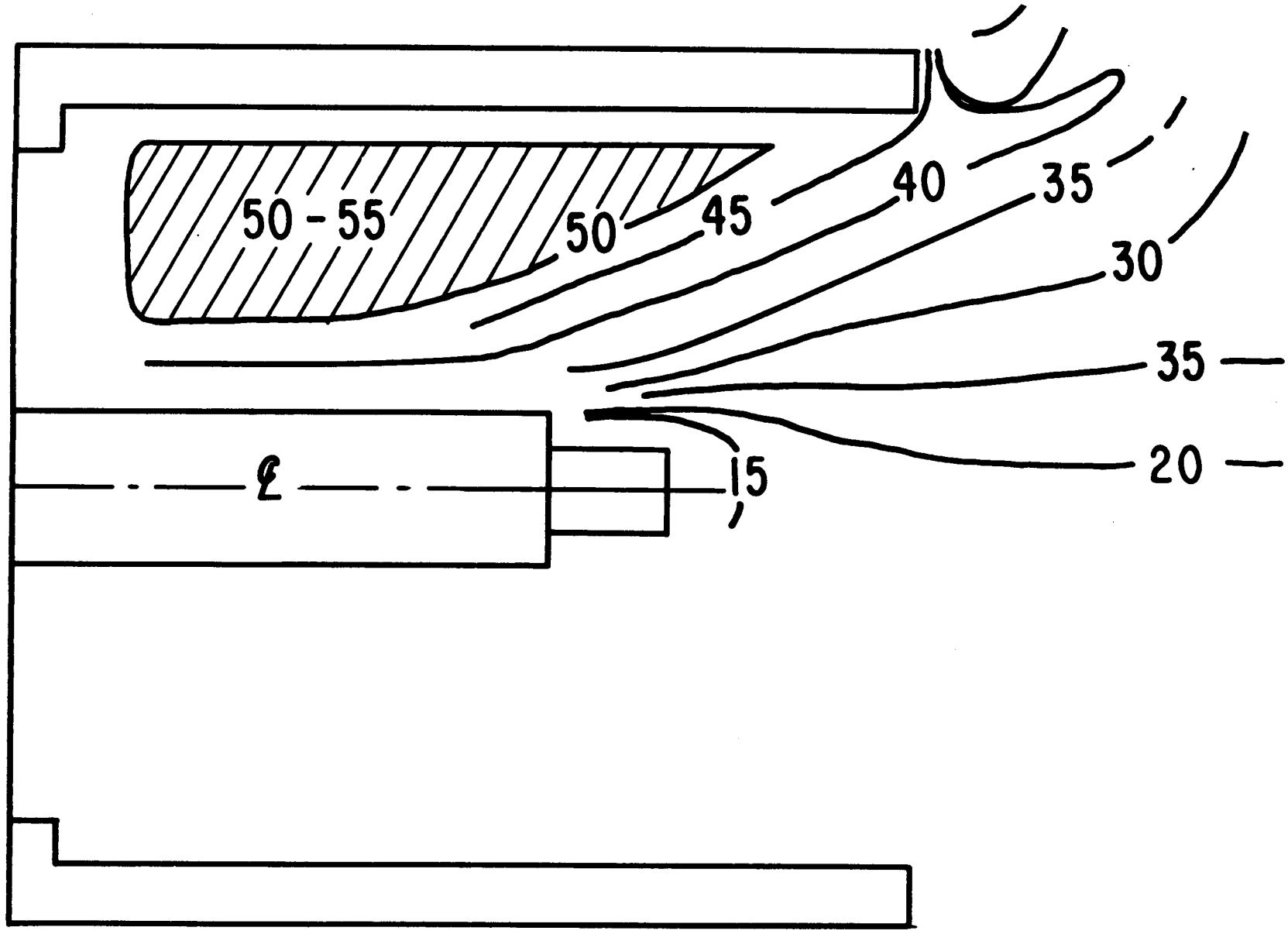

Fig. 18. Floating potentials in arc at the azimuth of the spoke.

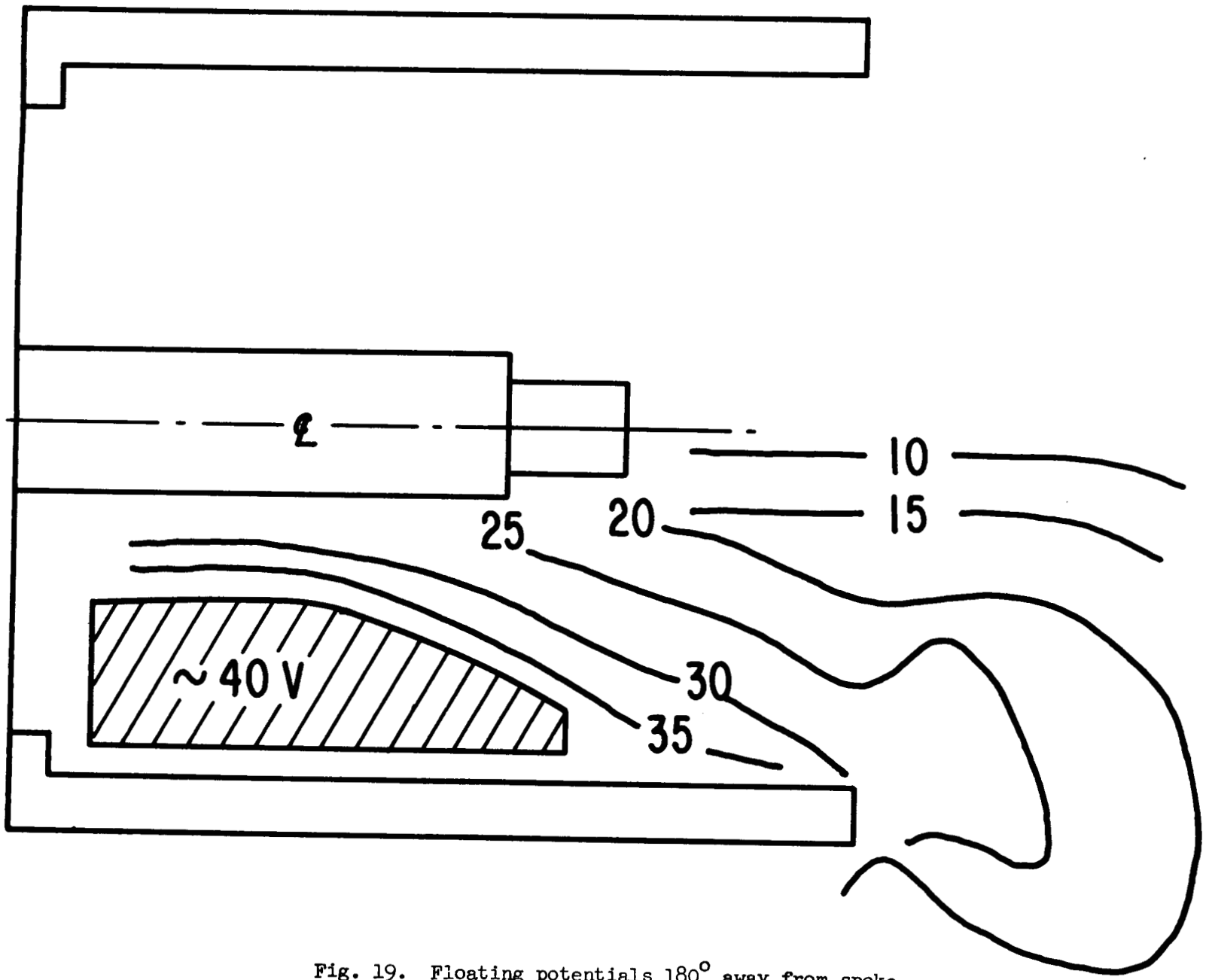

Fig. 19. Floating potentials 180° away from spoke.

So far, the output of this instrument has been contaminated by some extraneous noise, and has a somewhat inadequate frequency response, due to the high output impedance the collector must run into for adequate output. We expect to improve this situation by including an F. E. T. type of emitter follower within the probe and improving circuit shielding.

C Discussion

Since the experimental data so far obtained are incomplete, it is hazardous to attempt any general analysis of the arc operation; indeed, this may be an overly ambitious undertaking when our field maps are done. There are, however, some general conclusions one may reach on the basis of what information has been obtained.

First, it seems likely that the system is sustaining major losses of plasma through centrifugal "spinning" into the anode wall. Such a conclusion rests upon our observation that a radial Lorentz force component does not seem to exist, and this would be necessary to confine, radially, the plasma which has been given azimuthal velocity by the substantial $J_r B_z$ and $J_z B_r$. The rotating current column may or may not actually ionize and entrain the flowing neutral gas within itself; the the magnitude of E_θ, integrated across the width of the spoke, suggests that this actually does occur. Nevertheless, even if there is a relative azimuthal velocity between the plasma and the current distribution, the plasma necessarily possesses considerable angular velocity, and unless a radial component of $\vec{J} \times \vec{B}$ exists, losses to the wall would seem inevitable.

Secondly, it is clear that the acceleration process in this arc is <u>not</u> an interaction between an azimuthal Hall current and the radial component of the expanding bias field at the end of the accelerator. No net azimuthal current flows.

One might propose the hypothesis that the acceleration occurs through a two-stage process consisting of (1) a simple ionizing and heating of the gas by the radial discharge; followed by an expansion of this plasma in the "magnetic nozzle" formed by the bias coil field. This mechanism appears somewhat unlikely, however, for the following reason: One finds that the

gyro radius for any argon ion formed from rest in the combined E and B fields near the arc is much larger than the dimensions of the system, typically 24 cm or so. Thus, any nozzle expansion of the plasma must occur through first, an axial force

$$F_e = -\frac{W_\perp}{B} \nabla_\parallel B$$

being applied to the electrons, and then an electrostatic space-charge separation field being established to actually accelerate the ions. (This is necessary because the ions, to the extent that their gyro radii are very large compared to the system, are decoupled from the B field.) We note in Figures 18 and 19, however, that the electric field along B is very small; since our plot of B is as yet incomplete, we cannot state for certain that the B lines are exact equipotentials, but the shape of the potential contours suggests this quite strongly.

Against this argument, however, one may make the point that in order to have magnetic nozzle expansion in this instance, the integral of $E_\parallel$ along the field from the arc to infinity only has to equal the electron temperature; thus local $E_\parallel$ itself may be large enough for such expansion even though it is small compared to $E_\perp$, and, in the crude sort of visual comparisons we have done here, may be indistinguishable from zero. Further refinement of our field plots will be necessary in order to make a clear decision on this point.

Figure Captions

Fig. 1. Cutaway view of accelerator structure.

Fig. 2. View into muzzle of accelerator.

Fig. 3. Insulator and gas valve assembly.

Fig. 4. Cathode Ribbon and support structure.

Fig. 5. Rear of accelerator assembly, showing cathode heater transformer (bottom edge of picture) and a portion of the main pulse transformer (top of picture).

Fig. 6. Overall view of vacuum system.

Fig. 7. Interior of tank. The structure on the tank floor is the two-axis hydraulic probe carriage. The electrostatic beam analyzer is in the upper foreground.

Fig. 8. Electrical schematic of system, with delay sequence at lower left.

Fig. 9. Discharge current (upper traces) for line charging voltages of 2, 2.5, and 3 dv. Vertical, 1000 amperes/cm; horizontal, 100μs/cm.

Lower traces are discharge voltage (3 superimposed for the above charge voltages). Vertical, 50 v/cm.

Fig. 10. Arc voltage and current as a function of applied axial bias field. B_{zo} is the field beneath the coil at z = 0, the rear insulator. (cf. Fig. 11). The pulse line voltage is 1200 v for all points.

Fig. 11. Arc geometry, showing the coordinate system used in field mapping. The arrows show values of B_z at various positions for B_{zo} = 2200 gauss.

Fig. 12. Two traces each of $B_\theta(t)$ for z = 1.5 cm (near insulator) and z = 5.5 cm (near cathode).

Fig. 13. $J_r(t)$ traces for various r and z. The phase differences between different traces are not significant (see text).

Fig. 14. Rotation frequency as a function of arc current. B_{zo} = 2200 gauss.

Fig. 15. Rotation frequency as a function of B_{zo}.

Fig. 16. Muzzle region of accelerator, showing phase reference probe (L-shaped), together with differential E-probe.

Fig. 17. $E_\theta(t)$ in region of rotating spoke. Phase-probe triggering allows multiple-overlay data from single arc pulses.

Fig. 18. Floating potentials in arc at the azimuth of the spoke.

Fig. 19. Floating potentials 180^o away from spoke.

ERRATUM p.18

The argument given on the bottom of p.18 is in error, as may be seen by the following analysis of the generalized Ohm's law:

In general,

$$\vec{E} + \vec{v} \times \vec{B} - \frac{1}{n_e e}\left[\vec{j} \times \vec{B} - \nabla p_e\right] - \eta \vec{j} = 0$$

The azimuthal component of this relation is:

$$E_\theta - v_r B_z - \frac{1}{n_e e}\left[-j_r B_z - \frac{\partial p_e}{\partial \theta}\right] - \eta j_\theta = 0$$

where we neglect B_θ in comparison to B_z.

Assume azimuthal symmetry and steady state; then

$$E_\theta = \frac{\partial p_e}{\partial \theta} = 0 \; ; \quad \text{so}$$

$$j_r B_z = n_e e\left[v_r B_z + \eta j_\theta\right]$$

Assume also that the direct radial ion current is negligible, i.e., that $v_r \simeq 0$; then

$$j_r B_z = n_e e \eta j_\theta = \frac{j_\theta m}{e \tau_c} \; ; \quad \text{or,}$$

$$j_\theta / j_r = \frac{e B_z}{m} \tau_c = \omega \tau_c$$

as is well known.

The plasma thus experiences an azimuthal $\vec{j} \times \vec{B}$ acceleration component where momentum is transferred to ions through electron collisions, but where the electric field itself has no azimuthal component. ηj_θ does not equal E_θ, as implied in the text.

We are indebted to Dr. Jan Rosceszewski for bringing our attention to this point.